

Pressure-induced high-temperature superconductivity in ternary Y-Zr-H compounds

Wendi Zhao,¹ Defang Duan,^{2,*} Hao Song,¹ Mingyang Du², Qiwen Jiang², Tiancheng Ma², Ming Xu¹, and Tian Cui^{1,2,*}

¹*Institute of High Pressure Physics, School of Physical Science and Technology, Ningbo University, Ningbo 315211, China*

²*State Key Laboratory of Superhard Materials, College of Physics, Jilin University, Changchun 130012, China*

**Corresponding author.*

duandf@jlu.edu.cn

cuitian@nbu.edu.cn

Abstract: Compressed hydrogen-rich compounds have received extensive attention as appealing contenders for superconductors, and further challenges are maintaining the stability and superconductivity of hydrides at lower pressures. In this work, we found several novel hydrides YZrH₆, YZrH₈ and YZrH₁₂ with excellent superconductivity in the Y-Zr-H ternary system. Interestingly, YZrH₆ with an A15-type structure can maintain dynamic stability down to 0.01 GPa and still with a critical temperature (T_c) of 16 K. YZrH₈ and YZrH₁₂ have high T_c of 70 K and 183 K at 200 GPa and 160 GPa, respectively. The phonon modes associated with H atoms contribute significantly to the electron-phonon coupling, and the H-driven electronic density of states play an important role in superconductivity. These findings highlight relationship between the H-driven electronic density of states, electron-phonon coupling and the superconductivity in a distinct class of hydrides, opening new avenues for designing and optimizing new hydrogen-rich high temperature superconductors.

Keywords: high pressure, hydrides, superconductors, first-principles

1. Introduction

The lightest and most abundant element in nature is hydrogen, and the insulated hydrogen molecules were predicted to be able to transform into atomic metallic phase at sufficient high pressure¹. According to the Bardeen-Cooper-Schrieffer theory, atomic metallic hydrogen is considered as a potential room-temperature superconductor due to the high Debye temperature and strong electron-phonon coupling^{1, 2}. Although there have been many attempts to realize metallic hydrogen (pressures up to 500 GPa), the related reports are still controversial³⁻⁵. In 2004, it is proposed that introducing other elements into pure hydrogen to form hydrides can promote the transformation of the hydrogen into the metallic phase at low pressure, known as the effect of “chemical pre-compression”⁶. At present, almost all binary hydrides have been intensively studied in theoretical and a considerable part has been experimentally confirmed. For example, covalent hydride H₃S and clathrate hydrides CaH₆, YH₆, LaH₁₀, etc.⁷⁻¹³ all exhibit superconducting transition temperatures above 200 K. As is well known, the clathrate hydrides widely exist in alkaline earth and rare earth metal hydrides, and clathrate hydrides CaH₆ containing H₂₄ cage was predicted with remarkably high T_c of 220-235 K at 150 GPa¹¹. Its high T_c is attributed to the physical characteristics and properties of the clathrate hydrogen lattice close to the metallic hydrogen, and the Ca atoms as electron donors play an important role in stabilizing the H₂₄ cage. Recently, CaH₆ has been successfully synthesized and the measured superconducting critical temperature T_c is 215 K at 172 GPa¹⁴, which is in good agreement with the previous calculation. Furthermore, some hydrides with A15-type structures are also predicted to have high T_c , such as AlH₃, ZrH₃, MgSiH₆, LiPH₆, etc.¹⁵⁻²⁰, among which LiPH₆ is predicted to exhibit a high T_c of 167 K at 200 GPa¹⁸.

The fruitful results of searching for high-temperature superconductors in binary hydrides have promoted the relevant research of ternary hydrides which have more abundant stoichiometries and structures. Incorporating new elements directly into well studied binary hydrides is an effective way to construct ternary hydrides. The lithium-doped magnesium hydride MgH₁₆, which contains a lot of H₂ molecular units, and the introduction of extra electrons effectively promoted the dissociation of H₂ molecular

units, further forming $\text{Li}_2\text{MgH}_{16}$ with remarkably high estimated T_c of ~ 473 K at 250 GPa²¹. Another optimized strategy is engineering binary hydride backbones, which are easier to metallize than pure H backbones and can be designed by doping known structures with additional atoms, which break the local motif of the parent structure. For example, Zhang et al. theoretically predict that LaBeH_8 with a “fluorite-type” H-Be alloy backbones can maintain dynamic stability as low as 20 GPa and exhibit a high T_c of 185 K²². Notably, the superconductivity of some binary hydrides is well preserved by doping with Y element, such as ternary clathrate hydrides YCaH_{12} , LaYH_{12} , YLuH_{12} , etc²³⁻²⁷. Recently, a series of La-Y-H ternary compounds have been successfully synthesized recently²³. As is well known, Y and Zr atoms have similar electronegativity and atomic radius. High temperature superconductors are very likely to exist in ternary Y-Zr-H system.

We performed the systematical structure searches in the Y-Zr-H system under high pressure and discovered several novel hydrides: stable $Pm\bar{3}$ - YZrH_6 , $P4/mmm$ - YZrH_8 and metastable $Pm\bar{3}m$ - YZrH_{12} . $Pm\bar{3}$ - YZrH_6 has an A15-type structure. Both $P4/mmm$ - YZrH_8 and $Pm\bar{3}m$ - YZrH_{12} contain clathrate hydrogen sublattices. Electron-phonon coupling (EPC) calculations indicate that they are both potential high-temperature superconductors. Especially YZrH_6 can maintain dynamic stability down to 0.01 GPa, which is favorable for synthesis and applications at ambient pressure.

2. Computational methods

We performed the high-pressure structure searches of YZrH_x ($1 \leq x \leq 12$) with 1–2 formula units using AIRSS (Ab initio Random Structure Searching) code^{28, 29} at 200 GPa. A plane-wave cut-off of 500 eV and Monkhorst-Pack meshes k -point spacing of $2\pi \times 0.07 \text{ \AA}^{-1}$ were used. All predicted structures have been re-optimized by the on-the-fly (OTF) generation of ultrasoft pseudopotentials in CASTEP (Cambridge Sequential Total Energy Package) code³⁰, where the valence electrons configurations are $4s^2 4p^6 4d^1 5s^2$ for Y, $4s^2 4p^6 4d^2 5s^2$ for Zr and $1s^1$ for H. The Brillouin zone was sampled with a k -point mesh of $2\pi \times 0.03 \text{ \AA}^{-1}$, and the cut-off energy of 800 eV was chosen to ensure that the convergence of enthalpy within 1 meV/atom. Electronic properties were

calculated within the framework of density functional theory as implemented in Vienna ab initio simulation package (VASP)³¹. The Monkhorst-Pack k -mesh with grid spacing of $2\pi \times 0.02 \text{ \AA}^{-1}$ and energy cut-off of 1000 eV were adopted. The exchange-correlation functional was described using the Perdew-Burke-Ernzerhof (PBE) parametrization within the generalized gradient approximation (GGA). The ion-electron interactions part was implemented with the projector augmented wave (PAW) method³². The EPC matrix elements were calculated using density functional perturbation theory as implemented in the Quantum ESPRESSO package³³. The ultrasoft pseudopotential were selected with a kinetic energy cut-off of 80 Ry. A $24 \times 24 \times 24$ k -point grid and a $6 \times 6 \times 6$ q -point grid were chosen for YZrH_6 and YZrH_{12} . A $15 \times 15 \times 12$ k -point grid and a $5 \times 5 \times 4$ q -point grid were chosen for YZrH_8 . The Allen-Dynes modified McMillan equation³⁴ and Gor'kov-Kresin equation (G-K)³⁵ were used to calculate the superconducting critical temperature.

3. Results and discussion

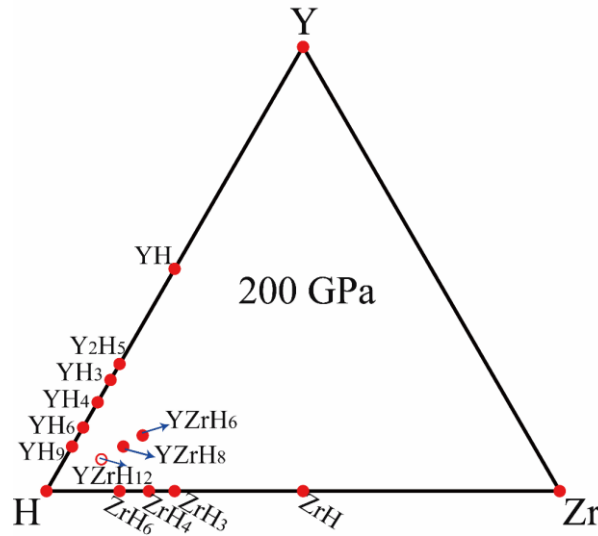


Fig.1 The ternary phase diagram (convex hull) of the Y-Zr-H system at 200 GPa. The red solid circles indicate stable structures, and the red hollow circles indicate metastable structures. The structures of stable element (Y, Zr and H) and binary compounds locating on the edges of the triangle were obtained from previous work^{15, 36-40}.

We performed structure searches in the ternary YZrH_x ($1 \leq x \leq 12$) system at 200 GPa. The thermodynamic stability of all predicted high-pressure structures was determined by constructing a ternary convex hull (see Fig.1). The results show that YZrH_6 and YZrH_8 fall on the convex hull, while the YZrH_{12} is 45 meV above the convex hull at 200 GPa, which is thermodynamic metastable. Considering that many metastable compounds have been synthesized experimentally in the inorganic crystal database^{41, 42}, YZrH_{12} still has the possibility of being synthesized in high-pressure experiments. As for YZrH_6 , there are two competitive phases $R\bar{3}$ and $Pm\bar{3}$, which have very close enthalpies (see Fig. 2a). Since highly symmetric structures tends to possess high-temperature superconductivity, the cubic $Pm\bar{3}$ phase will be the focus of our discussion.

We analyzed possible high-pressure synthesis routes for YZrH_6 , YZrH_8 and YZrH_{12} . It is reported that a series of Y-H compounds were synthesized using YH_3+H_2 or $\text{Y}+\text{H}_2$ as reactants⁴⁰, $Pm\bar{3}n\text{-ZrH}_3$ was synthesized using ZrH_2+H_2 or $\text{Zr}+\text{H}_2$ as reactants, and it remained stable above 10 GPa¹⁵. These results show that binary hydrides YH_3 , ZrH_3 , ZrH_2 and pure elements Y, Zr, H_2 are possible reactants. As shown in Fig. 2, we mainly calculated the formation enthalpies of YZrH_6 , YZrH_8 and YZrH_{12} relative to these reactants. YZrH_6 has a lower enthalpy of formation relative to multiple synthetic routes. Especially at ambient pressure, its significant energetic advantage over synthetic routes ($\text{Y}+\text{Zr}+\text{H}_2$ and $\text{Y}+\text{ZrH}_2+\text{H}_2$, etc.), means it is promising to be synthesized at ambient pressure. Relative to the different synthetic routes, YZrH_8 and YZrH_{12} have the lowest enthalpies above 140 GPa and 180 GPa, respectively, suggesting that they can be synthesized at high pressure. We further confirmed the dynamic stability of YZrH_6 , YZrH_8 and YZrH_{12} by calculating the phonon dispersion curves (see Fig. 6b and Fig. 7). The minimum stable pressures of YZrH_8 and YZrH_{12} are 200 GPa and 160 GPa, respectively. Surprisingly, YZrH_6 can maintain dynamic stable down to 0.01 GPa. In the following discussion, we will focus on their structure and properties at the lowest stable pressure.

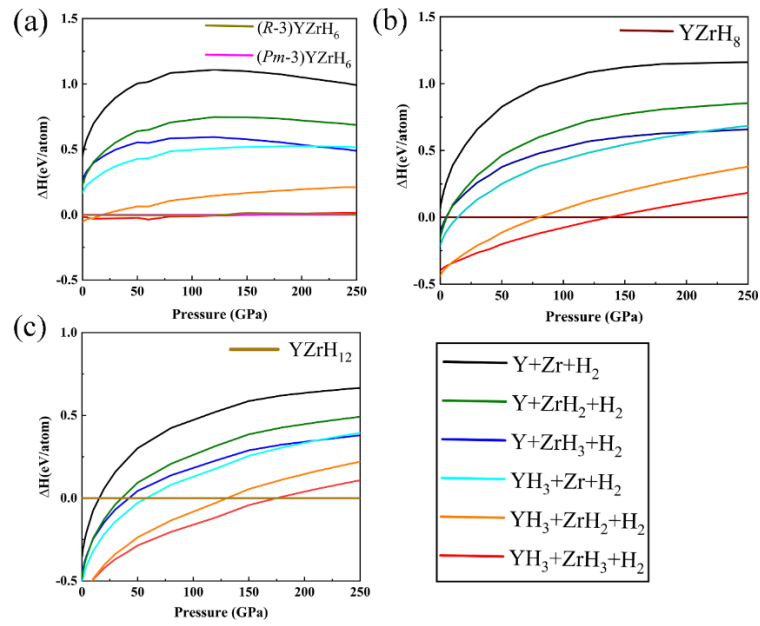


Fig. 2 The enthalpy difference curves with respect to (a) YZrH_6 , (b) YZrH_8 and (c) YZrH_{12} from divergent synthetic routes as a function of pressure.

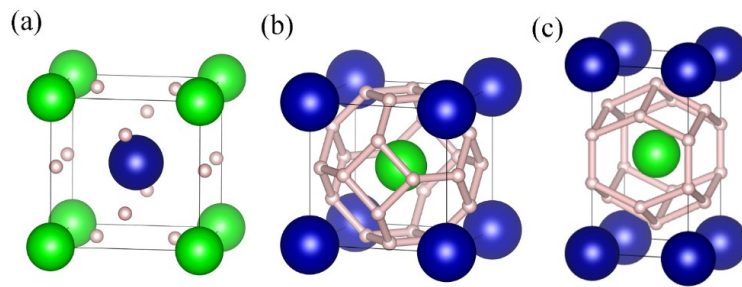


Fig.3 The crystal structure of (a) YZrH_6 at 0.01 GPa, (b) YZrH_{12} at 160 GPa and (c) YZrH_8 at 200 GPa. The blue, green, and pink spheres represent Y, Zr and H atoms, respectively.

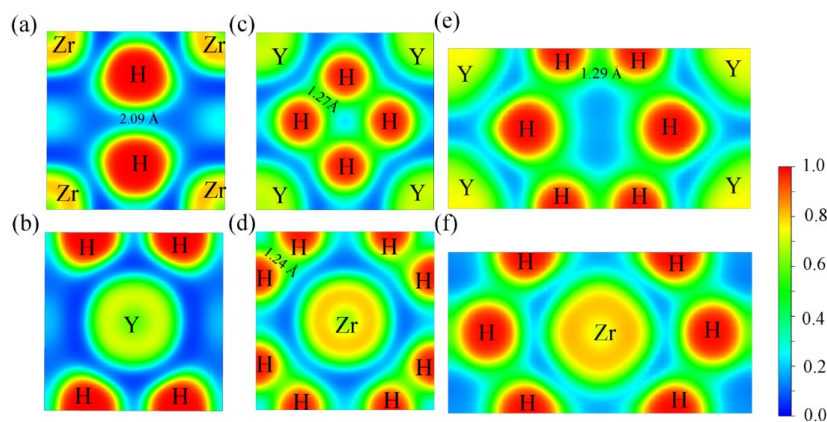


Fig.4 The electron localization functions of Y-H plane and Zr-H plane in (a-b) YZrH_6 at 0.01 GPa, (c-d) YZrH_{12} at 160 GPa and (e-f) YZrH_8 at 200 GPa.

The structure of $Pm\bar{3}$ -YZrH₆ is very similar to that of A15-type hydrides (AlH₃, GaH₃, ZrH₃, etc^{15, 19, 20}), the difference is that its metal atom positions are inequivalent, as shown in Fig. 3. For $Pm\bar{3}$ -YZrH₆, the Y and Zr occupy 1a (0.000, 0.000, 0.000) and 1b (0.500, 0.500, 0.500) sites, respectively, forming a cubic lattice. All equivalent H atoms occupy 6f (0.237, 0.000, 0.500) sites. The nearest H-H distance is 2.09 Å at 0.01 GPa, which is much longer than the bonding distance of H-H bond. As the case of $Pm\bar{3}m$ -YZrH₁₂, metal atoms Y and Zr also form a cubic lattice. The H atoms form the H₂₄ cage around the metal atoms, which consists of six quadrilaterals and eight hexagons. The H-H distance is 1.24 Å-1.27 Å at 160 GPa. Similar clathrate structures also appear in the previously reported ternary hydrides YCaH₁₂, LaYH₁₂, etc²³⁻²⁵. For $P4/mmm$ -YZrH₈, H atoms form H₁₈ cages around metal atoms, the H-H distance range is 1.29-1.49 Å at 200 GPa. Interestingly, YZrH₈ can also be obtained by substitution of binary hydrides $I4/mmm$ -YH₄ or $I4/mmm$ -ZrH₄^{39, 43, 44}. This indicates that elements with similar atomic radius and electronegativity may share the same hydrogen sublattice and further form new ternary hydrides.

The calculated electron localization function (ELF) and bader charge were used to analyze the electronic properties of YZrH₆, YZrH₁₂ and YZrH₈. The common feature is the low ELF values between the metal atoms and H, which confirm the existence of ionic bonds (see Fig. 4). It is worth noting that there is a low ELF value between the nearest H atoms in YZrH₆, which is consistent with the long H-H bond length, reflecting the ionic character of the structure. Bader charge analysis of YZrH₆ at 0.01 GPa shows that each Y and Zr atom loses charges of 1.73 and 1.69 |e|, respectively, and each H atom gains 0.57 |e| charges. Furthermore, the ELF values between the nearest-neighbor H-H in YZrH₁₂ and YZrH₈ are 0.6 and 0.5, respectively, indicating the formation of weak covalent bonds (see Fig. 4). Bader charge analysis reveals that each Y and Zr atom in YZrH₁₂ at 160 GPa transfer 1.39 and 1.47 |e| charges to the H atom, respectively, so that each H atom gains an average of 0.24 |e| charges. For YZrH₈, each Y and Zr atom loses 1.27 and 1.46 |e| charges at 200 GPa, respectively, and each H atom gains 0.34 |e| charges. Obviously, the Y and Zr atoms in YZrH₆, YZrH₁₂ and YZrH₈ are good electron donors, and the H-H bonds are elongated due to the extra electron occupying

its anti-bonding states. Notably, each H atom in YZrH_6 obtains the most electrons from Y and Zr, so it can remain stable in the form of atomization. In addition, there are weak covalent interactions between the H atoms in both YZrH_{12} and YZrH_8 , which are beneficial to enhance the hydrogen-derived electronic density of states at the Fermi level.

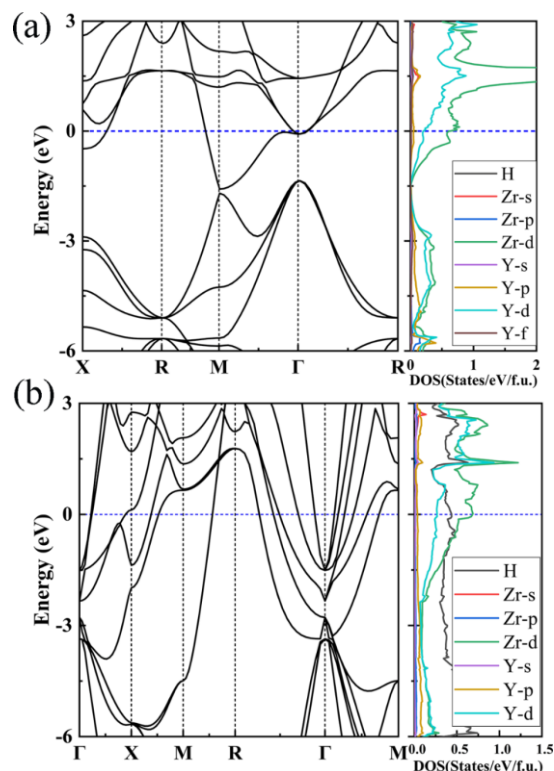


Fig. 5 Calculated electronic band structures and projected density of states (PDOS) for (a) YZrH_6 at 0.01 GPa (b) YZrH_{12} at 160 GPa. The Fermi level is set to zero.

The calculated electronic band structures and projected density of states of YZrH_6 and YZrH_{12} are shown in Fig. 5. The overlapping of valence and conduction bands indicates that they are metallic. For YZrH_6 , there are two obvious flat bands above the Fermi level about 1.5 eV, which are caused by the local d electrons of Y and Zr. They also further dominate the electronic density of states at the Fermi level. As the case of YZrH_{12} , many steep conduction bands cross the Fermi level around the Γ point and form multiple deep “electron pockets”. Note that high H-derived electronic density of states, which appearing near the Fermi level, is beneficial to strong electron-phonon coupling. As for YZrH_8 (see Fig. 6a), electron pockets near the Fermi level form around the Γ and R points while H has a significant contribution to the density of electronic

states at the Fermi level, these properties imply the potential superconductivity of the system.

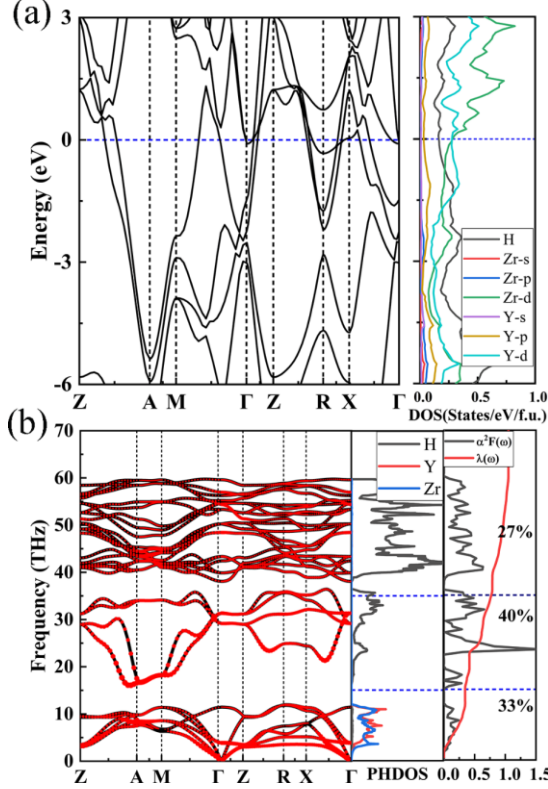


Fig. 6 (a) The electronic band structures and atom-projected density of states for $P4/mmm$ - $YZrH_8$ at 200 GPa. (b) Phonon dispersion curves, projected phonon density of states (PHDOS), and Eliashberg spectral function $\alpha^2 F(\omega)$ together with the electron-phonon integral $\lambda(\omega)$ for $P4/mmm$ - $YZrH_8$ at 200 GPa. The size of the red solid dots in the phonon spectra is proportional to the strength of electron-phonon coupling.

We further calculated the phonon dispersion curves, projected phonon density of states (PHDOS), Eliashberg spectral functions $\alpha^2 F(\omega)$ with the electron-phonon integral $\lambda(\omega)$ of $YZrH_8$, $YZrH_{12}$ and $YZrH_6$, as shown in Fig. 6b and Fig. 7. The phonon modes in the low frequency region are mainly associated with the Y and Zr atoms due to their heavy atomic masses. The lighter H atoms drive the phonon modes in the mid-high frequency region. Note that the high peaks of the Eliashberg spectral function $\alpha^2 F(\omega)$ appear in the middle frequency region, which are mainly caused by the soft phonon modes in this region. The soft phonon modes of $YZrH_8$ are distributed between 15 and 35 THz, contributing up to 40 % of the total λ (see Fig. 6b). For $YZrH_6$, the contribution of the soft phonon modes between 10 and 25 THz is also approximately

40 % (see Fig. 7a). At the same time, the phonon modes in the low-frequency region (< 10 THz) mainly related to Y and Zr atoms also have a significant contribution to the total λ up to 47 %. Interestingly, an appealing soft phonon mode in YZrH_{12} appears at the M point (see Fig. 7b), resulting in phonon modes in the mid-frequency (10-30 THz) region contributing as high as 48 % to the total λ . We use the size of the red dots on the phonon spectrum to represent the contribution of different phonon modes to the electron-phonon coupling, and find that the dense red dots are decorated on the soft phonon modes, indicating that they effectively enhance the electron-phonon coupling.

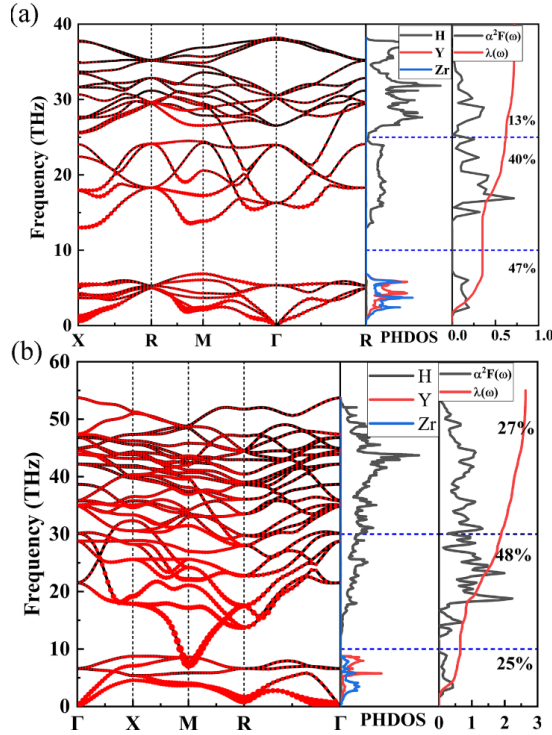


Fig.7 Calculated phonon dispersion curves, projected phonon density of states (PHDOS), and Eliashberg spectral function $a^2F(\omega)$ together with the electron-phonon integral $\lambda(\omega)$ for (a) $Pm\bar{3}$ - YZrH_6 at 0.01 GPa (b) $Pm\bar{3}m$ - YZrH_{12} at 160 GPa. The size of the red solid dots in the phonon spectra is proportional to the strength of electron-phonon coupling.

We evaluated the superconducting critical temperatures of YZrH_8 , YZrH_{12} and YZrH_6 by solving the Allen-Dynes modified McMillan equation:³⁴

$$T_c = \omega_{log} \frac{f_1 f_2}{1.2} \exp\left(\frac{-1.04(1+\lambda)}{\lambda - \mu^* - 0.62\lambda\mu^*}\right) \quad (1)$$

where f_1 and f_2 are two correction factors. The Coulomb pseudopotential μ^* is set to the typical 0.1-0.13. The logarithmic average phonon frequency ω_{log} and EPC parameter λ were given by:

$$\omega_{log} = \exp\left(\frac{2}{\lambda} \int \frac{d\omega}{\omega} \alpha^2 F(\omega) \ln(\omega)\right) \quad (2)$$

$$\lambda = 2 \int \frac{\alpha^2 F(\omega)}{\omega} d\omega \quad (3)$$

The calculated T_c of YZrH₈ at 200 GPa is 70-60 K. The λ and ω_{log} are 1.05 and 866.54 K, respectively. YZrH₁₂ exhibits the highest T_c 183-167 K at 160 GPa with λ and ω_{log} of 2.63 and 803 K, respectively. To evaluate the contribution of the optical branch of the phonon spectrum to the electron-phonon coupling, we calculated the T_c of YZrH₁₂ using the G-K equation³⁵, as shown in Fig.8a. The coupling constant λ_{opt} in the G-K equation is used to describe the interaction between electrons and optical phonons. The T_c obtained by solving the G-K equation at 160 GPa is 207 K. The increase in pressure reduces the density of states at the Fermi surface, thereby weakening the interaction of electrons with optical phonons, so the coupling constant λ_{opt} gradually decreases. The T_c value slightly decreases. In addition, the phonon frequency increases with increasing pressure, resulting in a larger ω_{log} . Therefore, there is no significant fluctuation of T_c under the competitive effect of ω_{log} and λ .

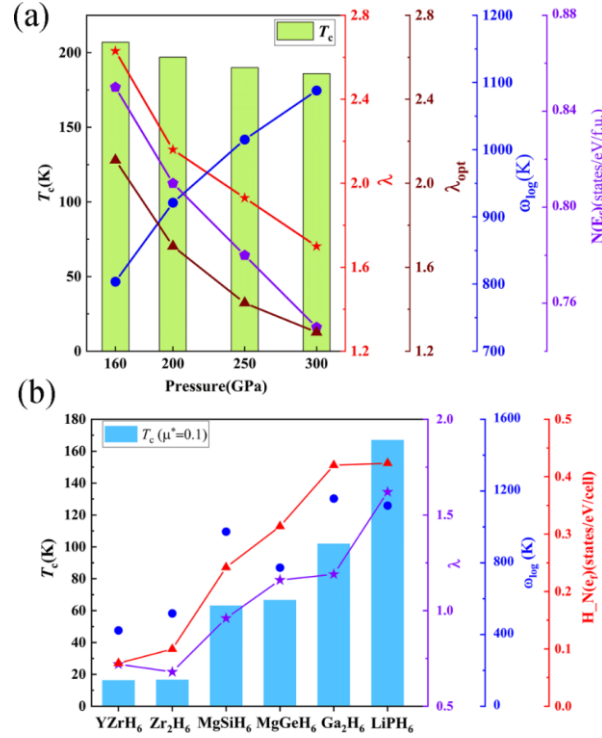


Fig. 8 (a) Calculated superconducting parameters of YZrH₁₂ at different pressures. The obtained T_c using GK equation ($\mu^* = 0.1$), strength of the interaction of electrons with optical phonons (λ_{opt}), electronic density of states at the Fermi energy (N_{ef}). (b) The T_c and related parameters of A15 hydrides. The superconducting parameters of ZrH₃, MgSiH₆, MgGeH₆, GaH₃ and LiPH₆ were obtained from previous work¹⁵⁻¹⁹. The T_{cs} are calculated using the Allen-Dynes modified McMillan equation ($\mu^* = 0.1$), and the DOS of hydrogen at the Fermi energy (H_N_{ef}).

The EPC constant λ and logarithmic average phonon frequency ω_{log} of YZrH₆ at 0.01 GPa are 0.72 and 423 K, respectively. Its T_c value reaches 16-13 K (see Fig. 8b). We further summarize the predicted T_c and related parameters of several A15-type hydrides in order to better explore the superconductivity of these hydrides, as shown in Fig. 8b. Obviously, the predicted T_c values generally increase with the density of states of hydrogen at the Fermi level and follow the same trend as electron-phonon coupling λ . H atoms drive the higher density of electronic states at the Fermi level and dominate phonon density of states, resulting in strong electron-phonon coupling. LiPH₆ not only has strong electron-phonon coupling, but also exhibits higher H_N_{ef} , and thus has highest T_c . Ternary A15-type hydrides are very abundant and have not been fully

explored. Choosing suitable elements to induce hydrogen-derived high electron density of states at the Fermi level is an effective strategy to obtain excellent superconductivity. Although YZrH_6 has a lower T_c , it remains stable at near-ambient pressures, which is beneficial for both experimental synthesis and practical applications.

4. Conclusions

In summary, we systematically investigated the structure and properties of ternary Y-Zr-H compounds under high pressure, and found stable YZrH_6 , YZrH_8 and metastable YZrH_{12} . YZrH_6 has an A15-type structure and maintain dynamic stability down to 0.01 GPa with T_c of 16 K. For this class of A15-type hydrides, the high contribution of hydrogen to the electronic density of states at the Fermi level is the key to induce high T_c . YZrH_8 and YZrH_{12} with clathrate hydrogen sublattices exhibit high superconducting transition temperatures of 70 K and 183 K at 200 GPa and 160 GPa, respectively. The soft phonon modes associated with the vibrations of hydrogen atoms in all three hydrides play an important role in enhancing the electron-phonon coupling. Our comprehensive analysis of the stability and superconductivity of Y-Zr-H compounds will motivate further theoretical and experimental studies.

Conflicts of interest

The authors declare no competing financial interest.

Acknowledgements

This work was supported by the National Key R&D Program of China (No. 2018YFA0305900), and the National Natural Science Foundation of China (Grants No. 52072188, No. 12122405, No. 51632002). Program for Changjiang Scholars and Innovative Research Team in University (Grant No. IRT_15R23), Some of the calculations were performed at the High Performance Computing Center of Jilin University and using TianHe-1(A) at the National Supercomputer Center in Tianjin.

References

1. N. W. Ashcroft, *Phys. Rev. Lett.*, 1968, **21**, 1748-1749.
2. J. Bardeen, L. N. Cooper and J. R. Schrieffer, *Phys. Rev.*, 1957, **106**, 162-164.
3. E. Wigner and H. B. Huntington, *J. Chem. Phys.*, 1935, **3**, 764-770.
4. V. L. Ginzburg, *J. Stat. Phys.*, 1969, **1**, 3-24.
5. M. I. Eremets, A. P. Drozdov, P. P. Kong and H. Wang, *Nat. Phys.*, 2019, **15**, 1246-1249.
6. N. W. Ashcroft, *Phys. Rev. Lett.*, 2004, **92**, 187002.
7. D. F. Duan, X. L. Huang, F. B. Tian, D. Li, H. Y. Yu, Y. X. Liu, Y. B. Ma, B. B. Liu and T. Cui, *Phys. Rev. B*, 2015, **91**, 180502.
8. D. F. Duan, Y. X. Liu, F. B. Tian, D. Li, X. L. Huang, Z. L. Zhao, H. Y. Yu, B. B. Liu, W. J. Tian and T. Cui, *Sci. Rep.*, 2014, **4**, 6968.
9. A. P. Drozdov, M. I. Eremets, I. A. Troyan, V. Ksenofontov and S. I. Shylin, *Nature*, 2015, **525**, 73-76.
10. M. Einaga, M. Sakata, T. Ishikawa, K. Shimizu, M. I. Eremets, A. P. Drozdov, I. A. Troyan, N. Hirao and Y. Ohishi, *Nat. Phys.*, 2016, **12**, 835-838.
11. H. Wang, J. S. Tse, K. Tanaka, T. Iitaka and Y. Ma, *Proc. Natl. Acad. Sci. U.S.A.*, 2012, **109**, 6463-6466.
12. Z. M. Geball, H. Liu, A. K. Mishra and M. Ahart, *Angew. Chem. Int. Ed.*, 2018, **57**, 688-692.
13. Z. Li, X. He, C. Zhang, X. Wang, S. Zhang, Y. Jia, S. Feng, K. Lu, J. Zhao, J. Zhang, B. Min, Y. Long, R. Yu, L. Wang, M. Ye, Z. Zhang, V. Prakapenka, S. Chariton, P. A. Ginsberg, J. Bass, S. Yuan, H. Liu and C. Jin, *Nat. Commun.*, 2022, **13**, 2863.
14. L. Ma, K. Wang, Y. Xie, X. Yang, Y. Wang, M. Zhou, H. Liu, X. Yu, Y. Zhao, H. Wang, G. Liu and Y. Ma, *Phys. Rev. Lett.*, 2022, **128**, 167001.
15. H. Xie, W. Zhang, D. Duan, X. Huang, Y. Huang, H. Song, X. Feng, Y. Yao, C. J. Pickard and T. Cui, *J Phys Chem Lett*, 2020, **11**, 646-651.
16. Y. Ma, D. Duan, Z. Shao, H. Yu, H. Liu, F. Tian, X. Huang, D. Li, B. Liu and T. Cui, *Phys. Rev. B*, 2017, **96**, 144518.
17. Y. Ma, D. Duan, Z. Shao, D. Li, L. Wang, H. Yu, F. Tian, H. Xie, B. Liu and T. Cui, *Phys Chem Chem Phys*, 2017, **19**, 27406-27412.
18. Z. Shao, D. Duan, Y. Ma, H. Yu, H. Song, H. Xie, D. Li, F. Tian, B. Liu and T. Cui, *npj Computational Materials*, 2019, **5**, 104.
19. G. Gao, H. Wang, A. Bergara, Y. Li, G. Liu and Y. Ma, *Phys. Rev. B*, 2011, **84**, 064118.
20. I. Goncharenko, M. I. Eremets, M. Hanfland, J. S. Tse, M. Amboage, Y. Yao and I. A. Trojan, *Physical Review Letters*, 2008, **100**, 045504.
21. Y. Sun, J. Lv, Y. Xie, H. Liu and Y. Ma, *Phys. Rev. Lett.*, 2019, **123**, 097001.
22. Z. Zhang, T. Cui, M. J. Hutcheon, A. M. Shipley, H. Song, M. Du, V. Z. Kresin, D. Duan, C. J. Pickard and Y. Yao, *Phys. Rev. Lett.*, 2022, **128**, 047001.
23. D. V. Semenov, I. A. Troyan, A. G. Ivanova, A. G. Kvashnin, I. A. Kruglov, M. Hanfland, A. V. Sadakov, O. A. Sobolevskiy, K. S. Pervakov, I. S. Lyubutin, K. V. Glazyrin, N. Giordano, D. N. Karimov, A. L. Vasiliev, R. Akashi, V. M.

- Pudalov and A. R. Oganov, *Mater. Today*, 2021, **48**, 18-28.
24. X. Liang, A. Bergara, L. Wang, B. Wen, Z. Zhao, X. F. Zhou, J. He, G. Gao and Y. Tian, *Phys. Rev. B*, 2019, **99**, 100505(R).
 25. H. Xie, D. F. Duan, Z. J. Shao, H. Song, Y. C. Wang, X. H. Xiao, D. Li, F. B. Tian, B. B. Liu and T. Cui, *J. Phys.: Condens. Matter*, 2019, **31**, 245404.
 26. W. Zhao, D. Duan, M. Du, X. Yao, Z. Huo, Q. Jiang and T. Cui, *Phys. Rev. B*, 2022, **106**, 014521.
 27. M. Du, H. Song, Z. Zhang, D. Duan and T. Cui, *Research*, 2022, **2022**, 9784309.
 28. C. J. Pickard and R. J. Needs, *Phys. Rev. Lett.*, 2006, **97**, 045504.
 29. C. J. Pickard and R. J. Needs, *J. Phys.: Condens. Matter*, 2011, **23**, 053201.
 30. M. D. Segall, P. J. D. Lindan, M. J. Probert, C. J. Pickard, P. J. Hasnip, S. J. Clark and M. C. Payne, *J. Phys.: Condens. Matter*, 2002, **14**, 2717-2744.
 31. A. Gk and B. Jf, *Comput. Mater. Sci.*, 1996, **6**, 15-50.
 32. J. P. Perdew, K. Burke and M. Ernzerhof, *Phys. Rev. Lett.*, 1996, **77**, 3865-3868.
 33. P. Giannozzi, S. Baroni, N. Bonini, M. Calandra, R. Car, C. Cavazzoni, D. Ceresoli, G. L. Chiarotti, M. Cococcioni, I. Dabo, A. Dal Corso, S. de Gironcoli, S. Fabris, G. Fratesi, R. Gebauer, U. Gerstmann, C. Gougoussis, A. Kokalj, M. Lazzeri, L. Martin-Samos, N. Marzari, F. Mauri, R. Mazzarello, S. Paolini, A. Pasquarello, L. Paulatto, C. Sbraccia, S. Scandolo, G. Sclauzero, A. P. Seitsonen, A. Smogunov, P. Umari and R. M. Wentzcovitch, *J. Phys.: Condens. Matter*, 2009, **21**, 395502.
 34. P. B. Allen and R. C. Dynes, *Phys. Rev. B*, 1975, **12**, 905-922.
 35. L. P. Gor'kov and V. Z. Kresin, *Rev. Mod. Phys.*, 2018, **90**, 011001.
 36. Y. Zhao, J. Zhang, C. Pantea, J. Qian, L. L. Daemen, P. A. Rigg, R. S. Hixson, G. T. Gray, Y. Yang, L. Wang, Y. Wang and T. Uchida, *Phys. Rev. B*, 2005, **71**, 184119.
 37. J. Buhot, O. Moulding, T. Muramatsu, I. Osmond and S. Friedemann, *Phys. Rev. B*, 2020, **102**, 104508.
 38. C. J. Pickard and R. J. Needs, *Nat. Phys.*, 2007, **3**, 473-476.
 39. K. Abe, *Phys. Rev. B*, 2018, **98**, 134103.
 40. P. Kong, V. S. Minkov, M. A. Kuzovnikov, A. P. Drozdov, S. P. Besedin, S. Mozaffari, L. Balicas, F. F. Balakirev, V. B. Prakapenka, S. Chariton, D. A. Knyazev, E. Greenberg and M. I. Eremets, *Nat. Commun.*, 2021, **12**, 5075.
 41. Y. Wu, P. Lazic, G. Hautier, K. Persson and G. Ceder, *Energy & Environmental Science*, 2013, **6**, 157-168.
 42. Y. Hinuma, T. Hatakeyama, Y. Kumagai, L. A. Burton, H. Sato, Y. Muraba, S. Imura, H. Hiramatsu, I. Tanaka, H. Hosono and F. Oba, *Nat. Commun.*, 2016, **7**, 11962.
 43. X. F. Li, Z. Y. Hu and B. Huang, *Phys Chem Chem Phys*, 2017, **19**, 3538-3543.
 44. Y. Li, J. Hao, H. Liu, J. S. Tse, Y. Wang and Y. Ma, *Sci. Rep.*, 2015, **5**, 9948.